ACS NANO

www.acsnano.org

ARTICLE

Integration of Bone-Targeted Delivery and Crosstalk Modulation of Liver-Bone Axis for Improved Osteoporosis Therapy

Yunhao You,[#] Shaoqiu Leng,[#] Jie Shi,[#] Han Yang, Mingzheng Chang, Qingliang Ma, Dapeng Zhang, Haochen Sun, Lianlei Wang,[*] Zhiliang Gao,[*] Jiwei Cui,[*] and Xinyu Liu[*]

Cite This: *ACS Nano* 2025, 19, 23955−23968

Read Online

ACCESS | Metrics & More | Article Recommendations | Supporting Information

ABSTRACT: **Nanomedicines hold great promise for the treatment of osteoporosis, while their nonspecific accumulation in the liver typically reduces the drug delivery efficacy. Herein, we report bone-targeted liposomes encapsulated with arginine and active ingredient for the treatment of osteoporosis. These liposomes are functionalized with active ingredient to enhance the bone-targeting capability. The delivered agents directly modulate osteoblasts, osteoclasts, and osteocytes, promoting bone formation and inhibiting bone resorption to counteract osteoporotic bone loss. In addition to targeted bone delivery, the inevitable hepatic accumulation of liposomes is strategically utilized to stimulate the hepatic secretion of lecithin-cholesterol acyltransferase (LCAT), which, in turn, promotes bone remodeling by engaging the liver-bone axis. This dual mechanism, which combines targeted bone delivery with beneficial off-target hepatic effects, synergistically enhances therapeutic outcomes. Our findings highlight a promising nanomedicine-based strategy that takes advantage of interorgan communication to optimize osteoporosis treatment.**

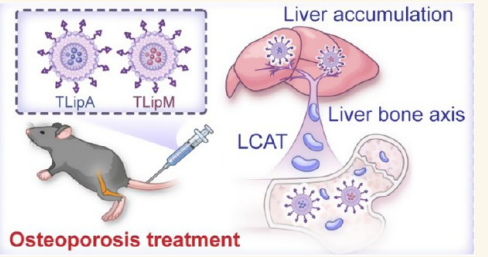

KEYWORDS: *nanomedicine, osteoporosis, liver-bone axis, bone-targeting, metabolic regulation*

INTRODUCTION

Osteoporosis is a systemic disease characterized by reduced bone mass, which results in decreased bone strength and significantly increases the risk of fractures.[1,2] With the global aging population, the incidence of osteoporosis is steadily increasing and becoming a significant public health concern.[3,4] Osteoporosis not only reduces the quality of life for patients but also places a substantial burden on the economy and healthcare systems due to its association with fragility fractures.[5,6] The current pharmacopeia for osteoporosis management primarily comprises two therapeutic classes: antiresorptives and osteoanabolic agents. Antiresorptive medications (e.g., selective estrogen receptor modulators, nitrogen-containing bisphosphonates, RANKL inhibitors) mitigate bone loss through potent suppression of osteoclast differentiation and activity. Conversely, osteoanabolic therapeutics (e.g., teriparatide [PTH(1−34)], romosozumab) exert bone-forming effects by stimulating mesenchymal stem cell lineage commitment toward osteoblastogenesis.[7,8] In contrast, anabolic drugs (e.g., teriparatide) stimulate osteoblast activity to promote bone formation and increase bone density.[9,10] While these therapies have achieved success in mitigating disease progression, their effectiveness is often limited by single-target mechanisms of action, suboptimal drug delivery efficiency, and off-target side effects.[11,12] Therefore, it is highly desirable to develop innovative therapeutic strategies to address the complex pathophysiology of osteoporosis.[13−15]

The pathogenesis of osteoporosis is inherently complex, involving intricate systemic interactions and metabolic imbalances.[16−18] Among these factors, the liver-bone axis has emerged as a critical pathway for bone metabolism regulation, which provides valuable insights for novel therapeutic development.[19,20] As the central organ in systemic metabolism, liver secretes numerous bioactive factors that significantly influence bone remodeling processes.[21,22] For instance, lecithin-cholesterol acyltransferase (LCAT) as a liver-derived enzyme plays a pivotal role in maintaining bone mass, where reduced expression of LCAT is associated with accelerated bone loss.[20,23] Furthermore, a recent study has demonstrated

Received: April 1, 2025
Revised: June 11, 2025
Accepted: June 11, 2025
Published: June 24, 2025

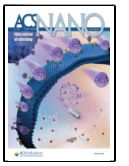

https://doi.org/10.1021/acsnano.5c05460
ACS Nano 2025, 19, 23955−23968

Scheme 1. Schematic Illustration of the Targeted Liposomes for the Treatment of Osteoporosis[a]

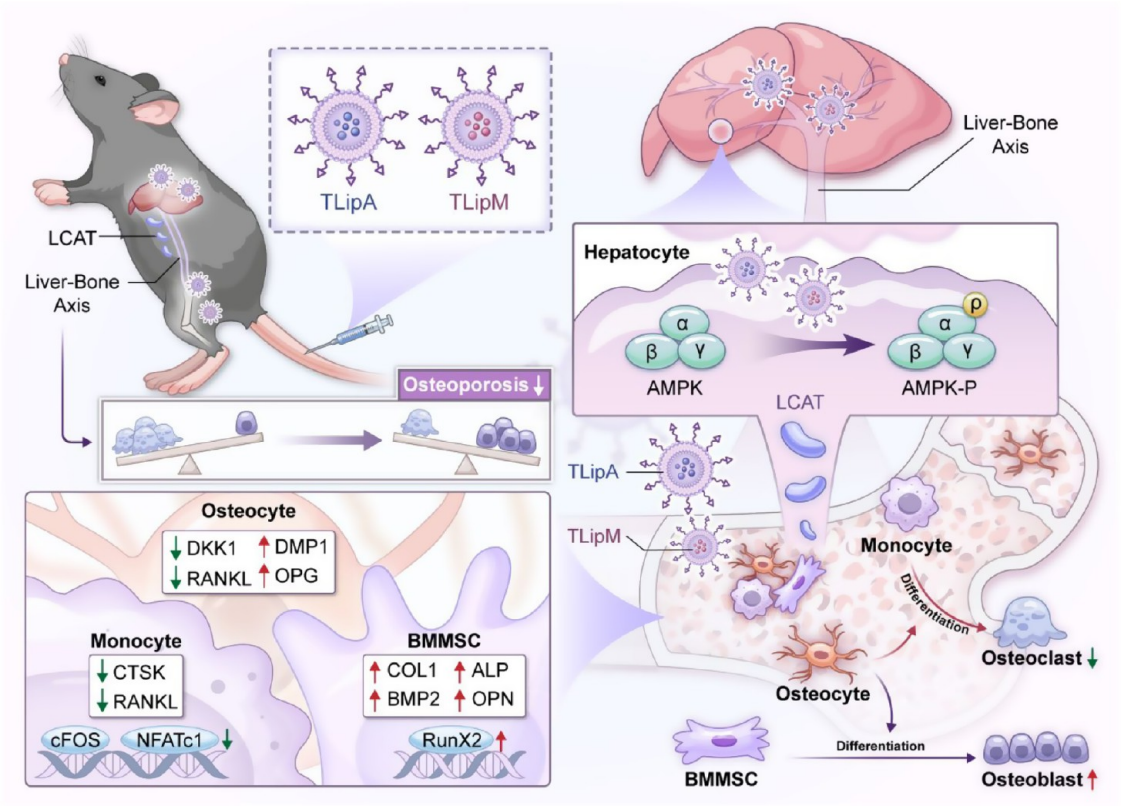

[a]The TLipA and TLipM can target bones for the delivery of arginine and active ingredient, while the off-targeted liposomes modulate liver-bone axis to promote osteogenesis and suppress osteoclastogenesis.

that liver-specific deficiency of SIRT2, a nicotinamide adenine dinucleotide (NAD+)-dependent deacetylase, suppresses osteoclastogenesis and effectively alleviates bone loss in osteoporosis.[19] These findings highlight the potential of the liver-bone axis in the pathophysiology of osteoporosis and provide opportunities for metabolically based therapeutic interventions. While compelling preclinical evidence has established the hepatic-osseous axis as a promising mechanistic framework for mitigating osteoporotic bone loss, the translational applications of this paradigm remain critically underexplored. Notably, the development of clinically viable therapeutic agents targeting this endocrine-metabolic crosstalk continues to represent a conspicuous void in the musculoskeletal pharmacopeia.

Nanomedicine-based drug delivery systems have attracted widespread attention for their potential to reduce the side effects of drugs and improve drug bioavailability.[24,25] The drug carriers can not only protect therapeutic agents from degradation but also deliver therapeutics to target sites,[26,27] which are promising for addressing the challenges associated with current osteoporosis therapy.[28,29] However, the clinical application of nanomedicines is hindered by several critical challenges.[30,31] The mononuclear phagocyte system (MPS) in the body rapidly recognizes and clears foreign nanomedicines from blood circulation, resulting in their accumulation in nontarget organs, such as the liver.[32,33] This unintended biodistribution significantly reduces the therapeutic concentration of drugs at target sites and raises safety concerns, including potential hepatotoxicity and systemic side effects.[33,34] Despite these limitations, the propensity of nanomedicines to accumulate in liver can be strategically exploited for therapeutic purposes.[35,36] The liver accumulation of nanomedicines is mainly applied in the treatment of liver diseases, while the use of liver accumulation to treat diseases of other systems is rarely reported.[37,38] By leveraging this phenomenon, nanomedicines could be designed to regulate the metabolism of the liver-bone axis, which thereby enhance bone remodeling. In this study, we reported the synthesis of bone-targeted liposomes loaded with arginine (denoted as TLipA) and active ingredient(denoted as TLipM for the treatment of osteoporosis (Scheme 1). L-Arginine, a conditionally dispensable amino acid, has garnered considerable attention for its dual regulatory capacity in osteogenic processes and hepatic homeostasis. Mechanistically, it enhances osteoblast mineralization capacity through nitric oxide synthase (NOS)-dependent pathways, while ameliorating bone loss and conferring hepatoprotection via urea cycle modulation. Active ingredient, acornerstone antidiabetic agent has evolved beyond glycemic control with demonstrated pleiotropic effects, particularly in enhancing hepatic active ingredient sensitivity and suppressing bone resorption through AMP-activated protein kinase (AMPK)-mediated osteoclast inhibition. These pharmacologically complementary mechanisms motivated the rational design of liposomes encapsulating both agents to potentiate their hepatoskeletal crosstalk targeting. The liposomes were functionalized with a bone-targeting molecule, active ingredient (ALN), to enhance the specificity of drug delivery at osteoporotic sites. This targeting strategy facilitates the accumulation of drugs in bone tissue, promoting osteogenesis and inhibiting osteoclast-mediated bone resorption. In

https://doi.org/10.1021/acsnano.5c05460
ACS Nano 2025, 19, 23955−23968

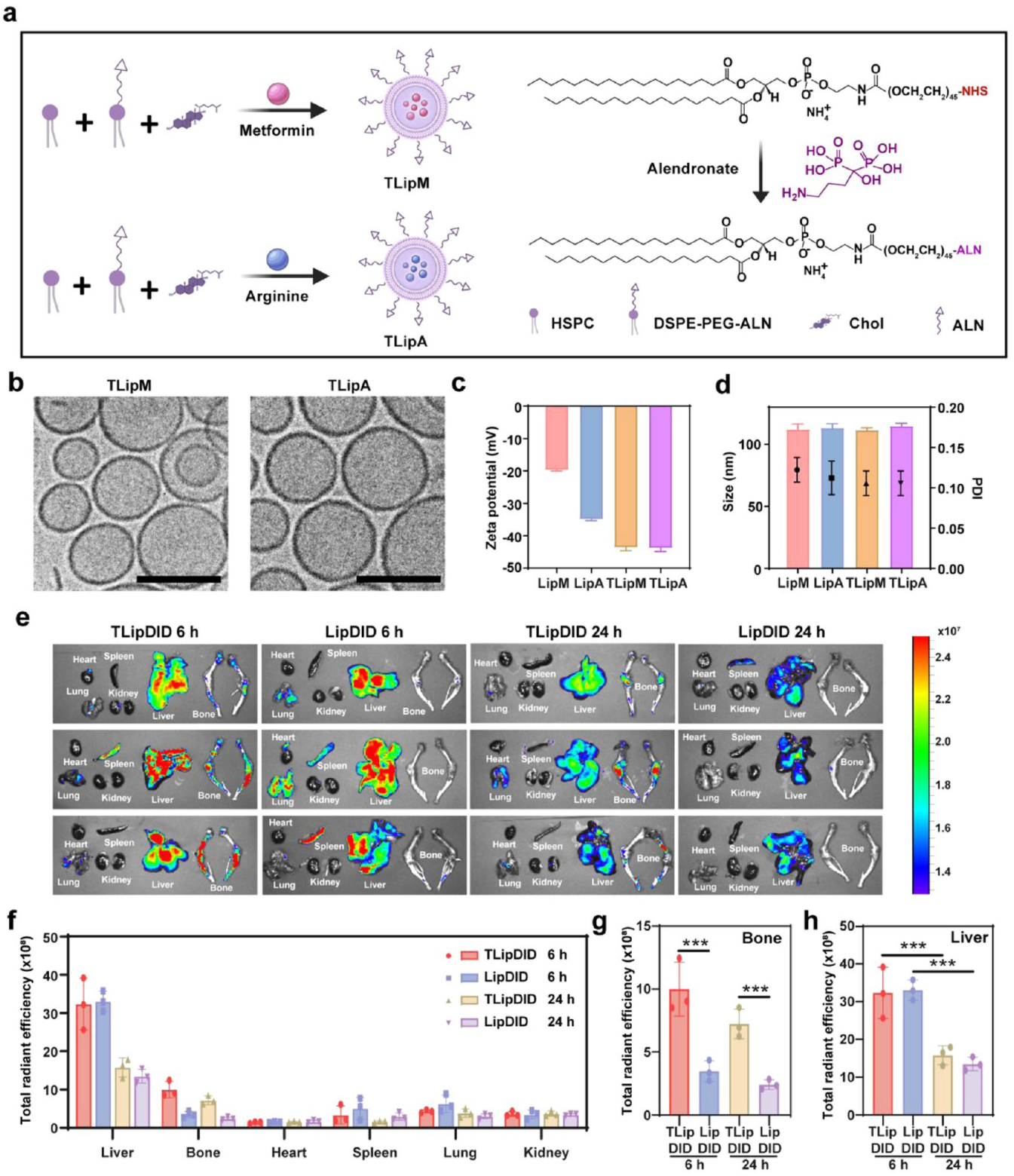

Figure 1. (a) Schematic illustration of the preparation of TLipM and TLipA. (b) Cryo-TEM images of TLipM and TLipA. Scale bars are 200 nm. (c) ζ-Potential and (d) size and PDI of LipM, LipA, TLipM, and TLipA. (e) Biodistribution of LipDID and TLipDID in heart, liver, spleen, lung, kidney, and bone at 6 and 24 h postinjection. (f) Total radiant efficiency of major organs and bones at 6 and 24 h postinjection (n = 3). (g, h) Comparison of total radiant efficiency of bone (g) and liver (h) after injection with LipDID or TLipDID at 6 and 24 h (n = 3). Data are presented as the mean ± SD, $^{**}P < 0.01$, and $^{****}P < 0.0001$.

addition to their bone-targeting capabilities, the liposomes also exploit the ineluctable liver accumulation. The encapsulated drugs (*i.e.*, arginine and active ingredient) regulate the metabolism of the liver-bone axis that influences bone remodeling and thereby achieve a synergistic effect for osteoporosis therapy. By combination of site-specific drug delivery with systemic

https://doi.org/10.1021/acsnano.5c05460
ACS Nano 2025, 19, 23955−23968

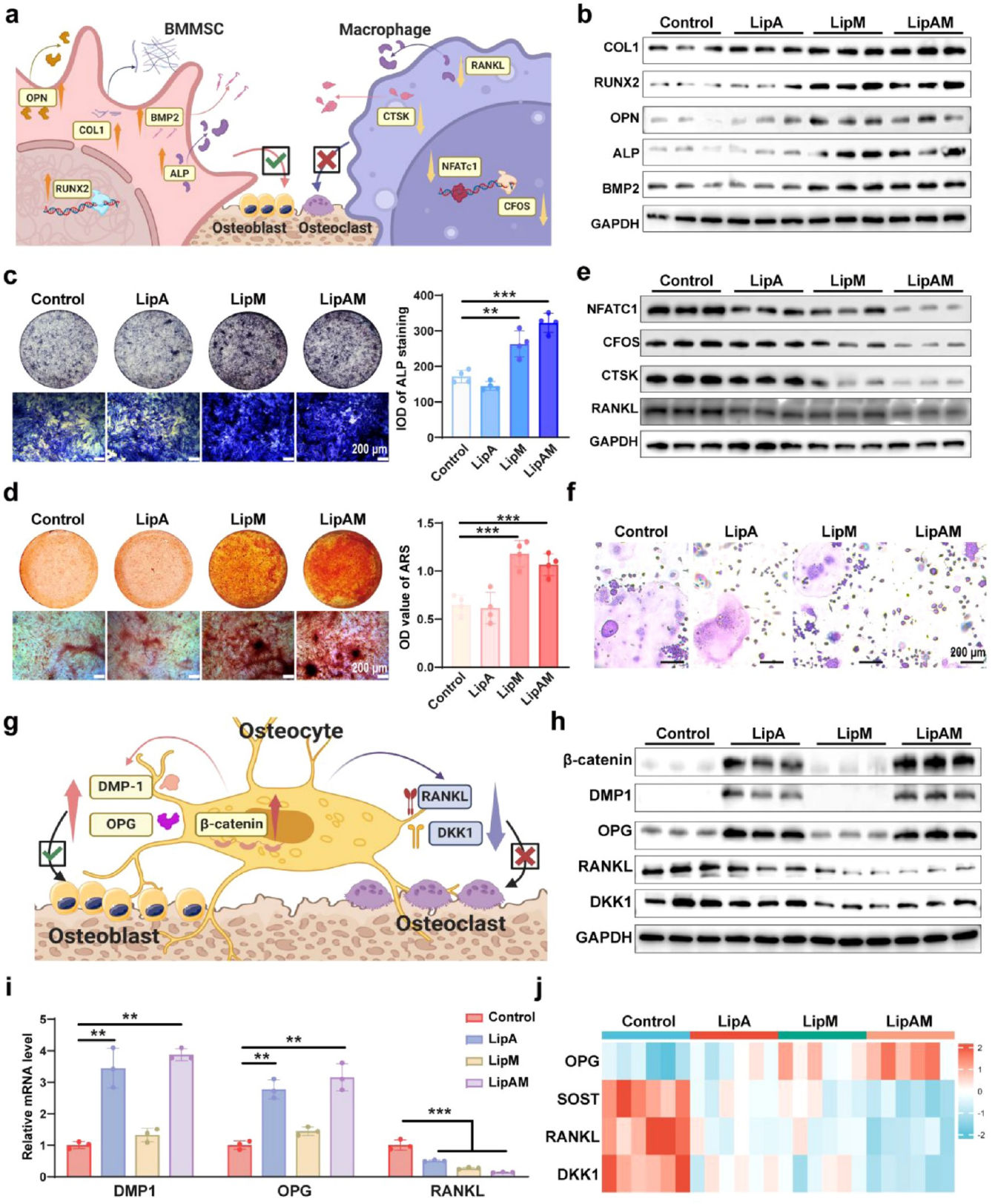

Figure 2. (a) Schematic representation illustrating the effect of LipAM on the promotion of osteogenesis and inhibition of osteoclasis in. (b) Protein expression levels of COL1, RUNX2, OPN, ALP, and BMP2 in BMMSCs on day 5 during osteogenic differentiation with different treatments. (c) ALP staining and quantitative results of BMMSCs after different treatments on day 14. Scale bars are 200 μm. (d) ARS and quantitative results of BMMSCs after different treatments on day 21. Scale bars are 200 μm. (e) Protein expression levels of RANKL, NFATC1, CSTK, and CFOS in RAW 264.7 on day 6 after different treatments. (f) TRAP staining images of osteoclasts on day 6 after RANKL and various treatments. (g) Schematic illustration of LipAM targeting osteocytes to promote osteogenesis and suppress osteoclastogenesis. (h) Western blotting assays for the β-catenin, DMP1, OPG, RANKL, and DKK1 expression in MLO-Y4 cells after

https://doi.org/10.1021/acsnano.5c05460
ACS Nano 2025, 19, 23955−23968

Figure 2. continued

treatments with LipA, LipM, or LipAM. (i) mRNA expression levels of DMP1, OPG, and RANKL of MLO-Y4 cells with different treatments. (j) ELISA assays for the OPG, SOST, RANKL, and DKK1 of culture supernatant of MLO-Y4 cells with different treatments.

metabolic regulation, the reported strategy transcends the limitations of conventional therapies, offering a comprehensive solution for the treatment of osteoporosis.

RESULTS AND DISCUSSION

Preparation and Characterization of Liposomes. Targeted liposomes loaded with active ingredient and arginine were prepared by using the film-dispersion method. The targeting molecule of ALN was conjugated to distearoyl-*sn*-glycero-3-phosphoethanolamine-PEG2000-*N*-hydroxysuccinimide (DSPE-PEG2000-NHS) prior to the liposome preparation to obtain DSPE-PEG-ALN (Figures S1 and S2). Liposomes were then fabricated with a molar ratio of 1,2-dipalmitoyl-*sn*-glycero-3-phosphocholine (DPPC), cholesterol, and DSPE-PEG2000-ALN at a mass ratio of 3:1:1. During the hydration process, active ingredient and arginine were encapsulated in the hydrophilic cavity of the liposomes (Figures 1a and S3) Liposomes loaded with active ingredient or arginine were defined as LipM and LipA, respectively. The morphology of TLipM and TLipA was observed using cryo-transmission electron microscopy (cryo-TEM), which revealed a hollow vesicle structure of the liposomes (Figure 1b). As shown in Figure 1c, the ζ-potentials of LipM and LipA were approximately −20 and −35 mV, respectively. After ALN modification, the ζ-potential of the liposomes decreased to approximately −43 mV, which was due to the negative charge of ALN. Dynamic light scattering (DLS) analysis indicated that the liposomes had an average diameter of ∼110 nm and a polydispersity index (PDI) of ∼0.1, indicating a homogeneous size distribution (Figure 1d). Additionally, after the incubation of TLipM and TLipA liposomes in DPBS for 7 days, no significant changes in particle size were observed, demonstrating their good stability (Figure S4).

Targeting and Biodistribution of Liposomes. Subsequently, the targeted and nontargeted liposomes were labeled with 1,1′-dioctadecyl-3,3,3′,3′-tetramethylindodicarbocyanine,4-chlorobenzenesulfonate Salt (DID) dye (denoted as TLipDID and LipDID, respectively) to investigate their targeting efficiency toward bone and liver using *ex vivo* imaging strategy. The distribution of TLipDID and LipDID in major organs and bone was evaluated at 6 and 24 h postinjection. *Ex vivo* imaging results demonstrated that TLipDID exhibited a markedly enhanced fluorescence signal in bone tissue at 6 h postinjection. In contrast, LipDID mainly accumulated in the liver, and weak signal was detected in bone tissue. At 24 h postinjection, the fluorescence signals of both TLipDID and LipDID in the liver and bone were reduced, indicating good metabolic clearance behavior (Figure 1e−h). Quantitative analysis of the liposome distribution ratio between bone and liver tissues was performed. The results showed that the bone-to-liver fluorescence ratios for the targeted and nontargeted nanoparticles were about 3:1 and 2.5:1 at 6 and 24 h postinjection, respectively (Figure S5). These findings further demonstrate that active ingredient modification significantly enhances the accumulation of the drugs in the bone tissue. The enhanced bone-targeting efficiency of the prepared liposomes is attributed to the surface modification with ALN. ALN selectively binds to hydroxyapatite in bone tissue, which increases the affinity of the liposomes for bone, leading to a higher accumulation in the bone compared to nontargeted liposomes.[39,40] For most nanomedicines, upon injection into the bloodstream, a protein corona is formed on the nanomedicines surface,[32,41] which can influence their *in vivo* behavior, facilitating recognition and clearance by the MPS. This process leads to the preferential accumulation of liposomes in liver.

Promotion of Bone Balance toward Osteogenesis. LipA and LipM were utilized to directly stimulate bone-related cells, including bone marrow mesenchymal stem cells (BMMSCs), osteoclasts, and osteoblasts, to assess their effects (Figure 2a). The results confirmed that both LipA and LipM significantly enhanced the osteogenic ability of mesenchymal stem cells. Quantitative Real-time PCR (qPCR) was used to confirm that the stimulation of LipM enhanced the expression of osteogenic-related mRNA containing type I collagen (*Col1*), alkaline phosphatase (*Alp*), osteopontin (*Opn*), runt-related transcription factor 2 (*Runx2*), and bone morphogenetic protein 2 (*Bmp2*) (Figure S6). Western blot experiments showed that LipM and LipA promoted the expression of osteogenic marker protein COL1, while LipM significantly enhanced the expression of RUNX2, OPN, ALP, and BMP2 compared to LipA (Figures 2b and S7). In the previous study, L-arginine did not significantly influence the biological functions of BMMSCs, as evidenced by osteoblast-related marker assays,[17,42,4]while the active ingredient was shown to influence the osteogenic process.[44−46] The combination therapy using LipM and LipA (LipAM) exhibited a significant improvement in osteogenic mRNA and protein expression. To verify the long-term effects of osteogenic differentiation, ALP staining on day 14 and alizarin red S (ARS) staining on day 21 were performed. The results showed that LipM and LipAM significantly enhanced the ALP enzyme activity and calcium salt accumulation ability of BMMSCs (Figure 2c,d). These findings suggest that LipAM stimulation notably improved the osteogenic differentiation potential of the BMMSCs.

To assess the *in vitro* effect of LipA and LipM on osteoclastogenesis, osteoclast differentiation was induced with RANKL in the presence of LipA or LipM. mRNA was extracted for qPCR analysis and proteins were obtained for Western blotting (WB) analysis on day 6. Both qPCR and WB showed that LipA and LipM significantly reduced the mRNA and protein expression of key osteoclast markers included nuclear factor of activated T cells 1 (NFATc1), CFOS, cathepsin K (CSTK), and receptor activator of nuclear factor-κB ligand (RANKL). Notably, the combination of LipA and LipM had the most significant effect on the inhibition of osteoclastic differentiation (Figures 2e, S8, and S9). Tartrate-resistant acid phosphatase (TRAP) staining indicated that LipAM exerted its suppressive role of osteoclast formation compared to LipA and LipM (Figures 2f and S10).

Osteocytes, the predominant cell type in bone matrix, secrete regulatory cytokines such as RANKL, osteoprotegerin (OPG), dickkopf-related protein 1 (DKK1), and sclerostin (SOST), thereby coordinately regulating the biological activity of osteoblasts and osteoclasts.[43,47] Osteocytes can affect the

https://doi.org/10.1021/acsnano.5c05460
ACS Nano 2025, 19, 23955−23968

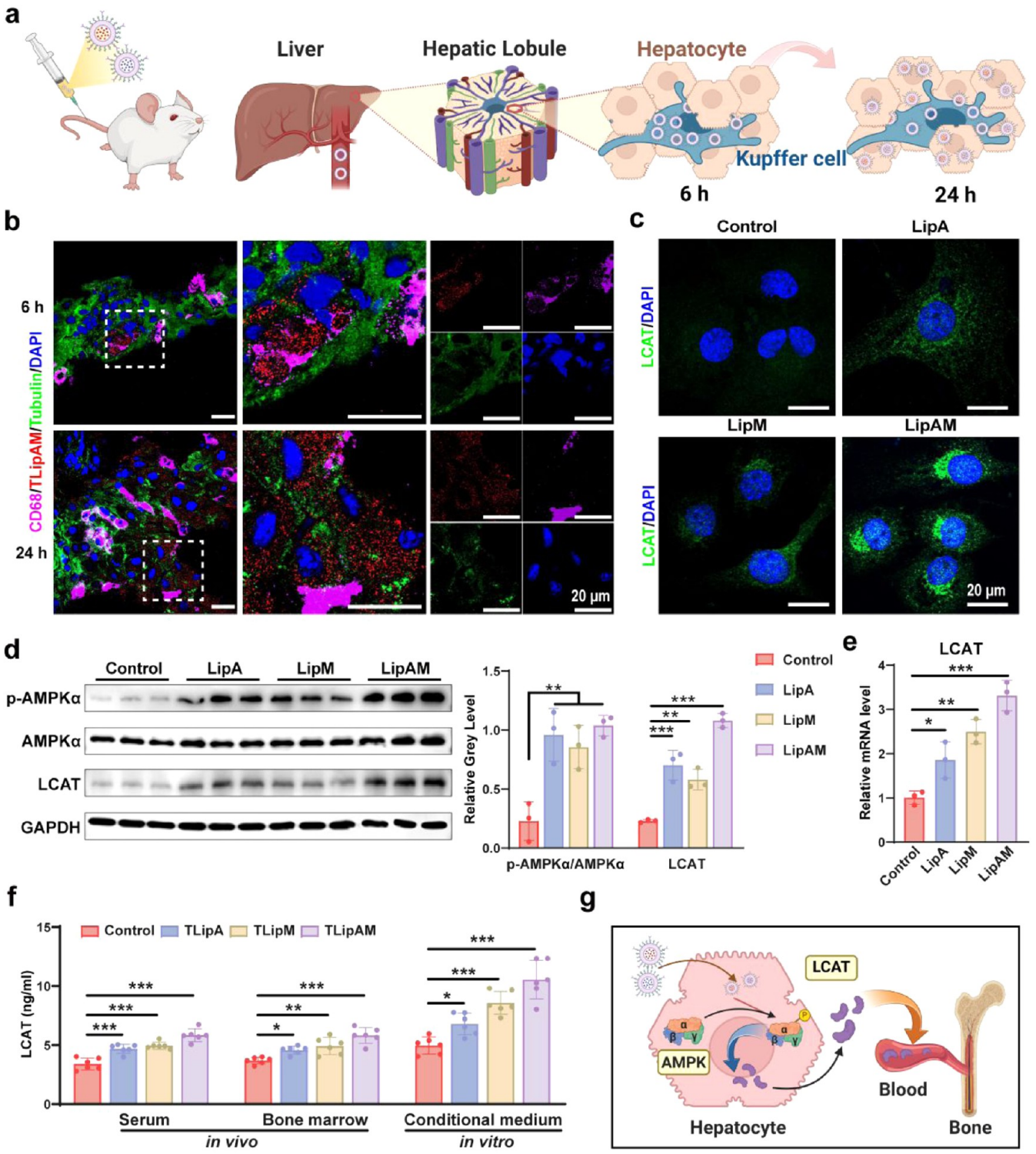

Figure 3. (a) Schematic diagram showing the biodistribution of TLipAM in liver. (b) Immunofluorescence staining images of liver tissues at 6 and 24 h postinjection. Scale bars are 20 μm. (c) Immunofluorescence staining images of LCAT in hepatocytes under different treatments. Scale bars are 20 μm. (d) Western blotting assays and quantitative results for the p-AMPKα, AMPKα, and LCAT expression in hepatocytes after incubation with LipA, LipM, and LipAM, respectively. (e) mRNA expression levels of LCAT of hepatocytes with different treatments. (f) ELISA assays for LCAT in blood serum and bone marrow *in vivo*, and supernatant medium of hepatocytes *in vitro*. (g) Schematic diagram showing the effect of TLipAM on the AMPK pathway of hepatocytes in liver.

balance between bone formation and bone destruction. Therefore, the effects of LipA and LipM on osteocytes were subsequently explored (Figure 2g). Treatment with LipA enhanced the gene and protein expression of key osteogenic-promoting cytokines related to osteocytes, including Dentin Matrix Acidic Phosphoprotein 1 (DMP1), β-catenin, and OPG (Figures 2h,i, S11, and S12). Simultaneously, it downregulated the gene and protein expression of osteoclast-promoting related cytokines RANKL and DKK1. In contrast, LipM did not significantly promote osteogenic-related proteins, including

https://doi.org/10.1021/acsnano.5c05460
ACS Nano 2025, 19, 23955−23968

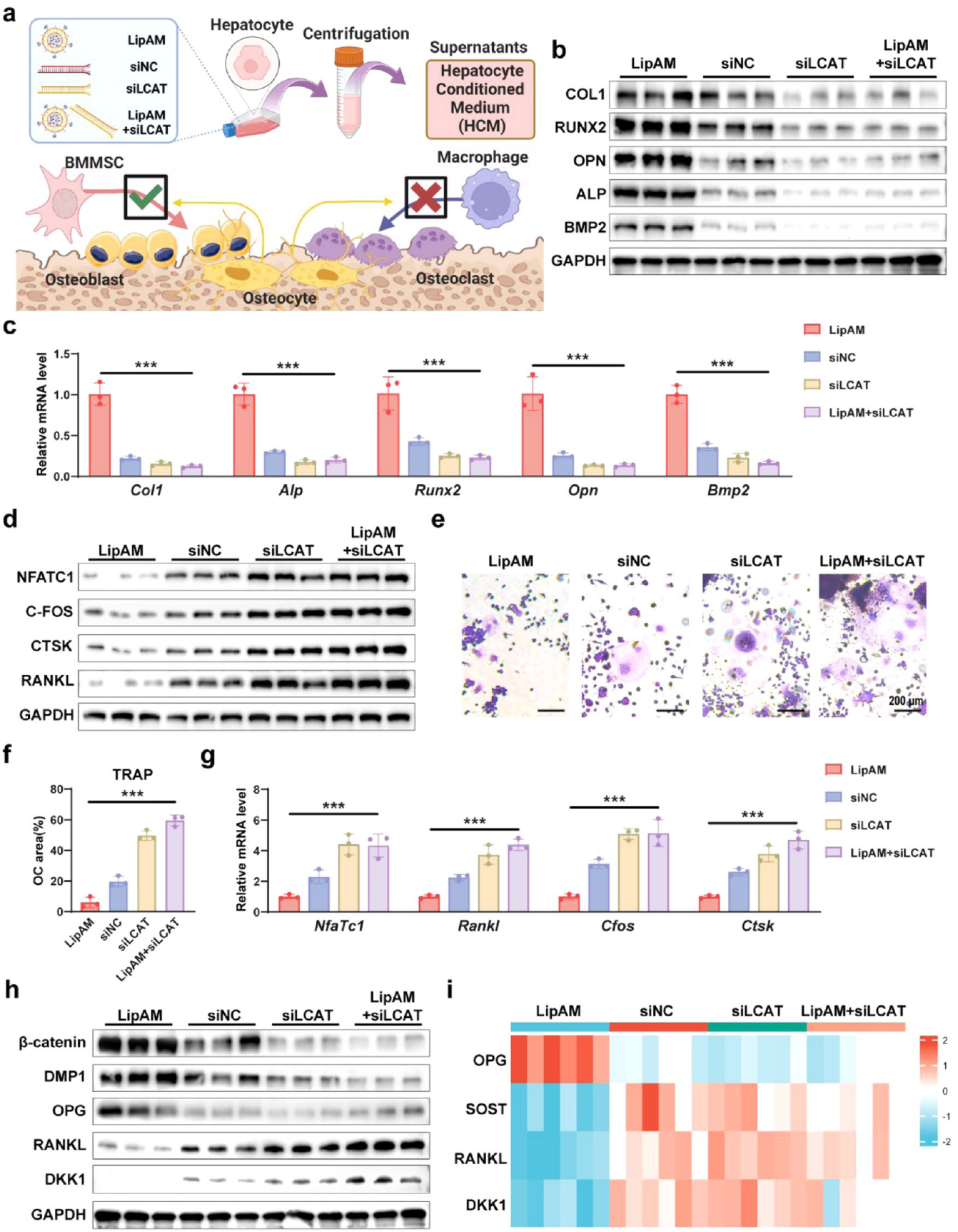

Figure 4. (a) Schematic diagram showing that siLCAT weakens the effect of LipAM liposomes on the promotion of osteogenesis and inhibition of osteoclasis in BMMSCs, monocytes, and osteocytes. (b) Protein expression levels of COL1, RUNX2, OPN, ALP, and BMP2 in BMMSCs on day 5 during osteogenic differentiation under different treatments of LipAM, siNC, siLCAT, or LipAM+siLCAT in HCM. (c) mRNA expression levels of *Col1, Runx2, Opn, Alp*, and *Bmp2* on day 3 during osteogenic differentiation after different treatments. (d)

https://doi.org/10.1021/acsnano.5c05460
ACS Nano 2025, 19, 23955−23968

Figure 4. continued

Protein expression levels of RANKL, NFATC1, CSTK, and CFOS in RAW 264.7 on day 6 cultured under differential HCM conditions (LipAM, siNC, siLCAT, and LipAM+siLCAT). (e) TRAP staining images of osteoclasts and (f) quantitative results for RAW 264.7 cultured under differential HCM conditions on day 6. Scale bars are 200 μm. (g) mRNA expression levels of *NfaTc1, Cfos, Rankl,* and *Ctsk* on day 6 cultured under differential HCM conditions. (h) Western blotting assays for the β-catenin, DMP1, OPG, RANKL, and DKK1 expression in MLO-Y4 cells after different treatments. (i) ELISA assays for the OPG, SOST, RANKL, and DKK1 of MLO-Y4 cells after different treatments.

DMP1, β-catenin, and OPG (Figures 2h,i, S11, and S12). However, LipM significantly inhibited the gene and protein expression of osteoclast-promoting related cytokines RANKL and DKK1, indicating distinct effects from LipA (Figures 2h,i, S11, and S12). The combination of LipA and LipM demonstrated the most pronounced effects in regulating osteogenic and osteoclast differentiation factors, promoting osteogenic differentiation and inhibiting osteoclast differentiation. Immunofluorescence analysis of β-catenin in bone cells revealed that both LipM and LipAM stimulated β-catenin expression (Figure S13). Given that osteocytes regulate the function of osteoblasts and osteoclasts through cytokine secretion, the changes in bone-cell-related proteins were indicative of corresponding alterations in osteocyte regulatory activity. To further validate these effects, ELISA assays were conducted to measure the levels of OPG, SOST, RANKL, and DKK1. Among the cytokines, osteogenic differentiation-stimulating OPG was significantly increased by LipM and LipAM treatments. Conversely, the osteoclast differentiation-related SOST, RANKL, and DKK1 were significantly inhibited under the stimulation of LipA and LipM, where the LipAM group showed more obvious inhibition (Figures 2j and S14). Therefore, LipA and LipM directly promote osteogenic differentiation of mesenchymal stem cells and inhibit osteoclast differentiation. Additionally, these treatments regulate osteogenic and osteoclast differentiation by modulating osteocyte function. LipAM group can further enhance the regulation of osteocytes, favoring osteogenic differentiation and inhibiting osteoclast differentiation.

Promotion of LCAT Secretion. To further investigate the transport and metabolism of liposomes in liver, fluorescence staining of liver tissue was performed at 6 and 24 h postinjection. The results revealed that TLipAM (*i.e.*, TLipA and TLipM) primarily accumulated around the Kupffer cells in the liver at 6 h. However, the distribution of liposome was found to be widespread throughout the liver at 24 post-injection, which demonstrates that targeted liposomes can enter hepatocytes and exert its effects (Figure 3a,b). Notably, LCAT is a liver-secreted hormone, and the liver can specifically secrete LCAT to regulate peripheral tissues.[48,49] LCAT has been shown to inhibit osteoclast maturation while enhancing osteoblast viability.[20] Immunofluorescence staining confirmed that TLipAM treatment significantly increased LCAT expression in hepatocytes (Figure 3c). qPCR further validated that TLipAM upregulated the mRNA expression of LCAT (Figure 3e). The system utilized the role of LCAT as a regulator for both bone and liver functions.

Previous studies have already proven that active ingredient is a potent AMPK pathway agonist.[50−52] However, whether arginine can activate the hepatic cell AMPK pathway has not yet been explored. Therefore, the degree of phosphorylation of AMPKα was assessed by WB, confirming that both active ingredient and arginine promoted AMPKα phosphorylation (Figure 3d). It is noteworthy that the corresponding increase in AMPKα phosphorylation is the increase in LCAT expression, suggesting that the production of LCAT is closely related to phosphorylation of AMPKα.[53] In addition, AMPK-IN-3 (characterized as a potent and selective AMPK inhibitor) was used to elucidate the molecular mechanism of LCAT biosynthesis upregulation caused by LipAM. As a result, AMPK inhibition directly abolished the ability of LipAM to promote LCAT expression in hepatocytes. These results confirmed that LipAM enhanced LCAT production through the activation of the AMPK pathway (Figure S15). The combination therapy using TLipM and TLipA is denoted as TLipAM. The examination of the hepatocyte culture supernatants showed that TLipAM stimulation induced the secretion of LCAT by hepatocytes. After injection of liposomes into rats, the serum and bone marrow LCAT contents were examined at 24 h, and the results showed that the administration of LipAM significantly increased the serum LCAT level and was able to transfer LCAT to the bone marrow, increasing the bone marrow LCAT level (Figure 3f). Emerging evidence suggests hepatic regulation of bone mass through IGF-1 signaling. To mechanistically disentangle whether LipAM interferes with the endocrine axis, serum IGF-1 levels at 24 h postinjection were quantified using ELISA. As a result, administration of LipAM did not induce significant alterations in IGF-1 expression, thereby validating the specificity of LipAM in enhancing LCAT activity rather than modulating IGF-1-mediated pathways (Figure S16). Consequently, TLipAM could enter the liver and activate the AMPK pathway of hepatocytes to produce LCAT and increase its level in both the blood and bone marrow (Figure 3g).

Regulation of the Liver-Bone Axis. To further investigate whether hepatocytes stimulated by LipAM exert their effects through LCAT or other key factors in promoting osteogenesis, hepatocyte conditional medium (HCM) stimulated by LipAM (LipAM HCM) was collected and added to the culture medium of osteoblasts, osteoclasts, and osteocytes (Figure 4a). To clarify the role of LCAT, siRNA of LCAT (siLCAT) and control (siNC) were used to interfere with the production of LCAT in hepatocytes. The experimental results confirmed that LipAM HCM induced the mRNA and protein expression of osteogenesis-related genes (Figures 4b,c and S17), enhanced ALP activity, and promoted calcium nodule formation (Figures S18 and S19), which indicated that LipAM HCM enhanced osteogenic differentiation. Regarding osteoclastic differentiation, the mRNA and protein of osteoclast-related genes (Figures 4d,g and S20) and TRAP staining were weakened (Figure 4e,f), indicating that LipAM HCM led to osteoclastic differentiation inhibition. PCR, WB, and ELISA proved that LipAM HCM could induce osteocytes to promote osteogenic differentiation while inhibiting osteoclastic differentiation (Figures 4h,i and S21).

siLCAT was used to inhibit the production of LCAT in hepatocytes, and then, LipAM was stimulated the hepatocytes with LipAM again to extract the supernatant (LipAM +

https://doi.org/10.1021/acsnano.5c05460
ACS Nano 2025, 19, 23955−23968

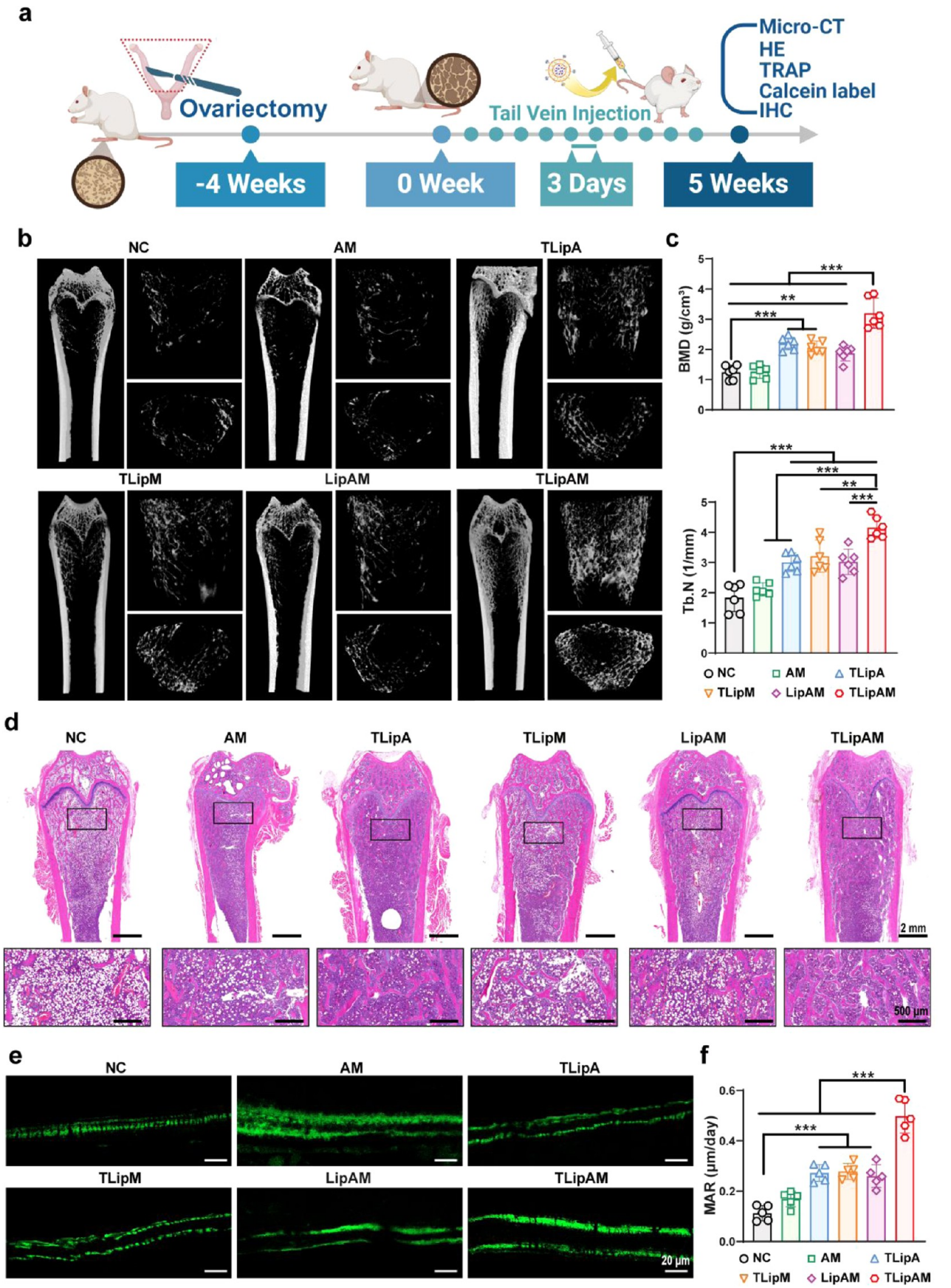

Figure 5. (a) Experimental schedule to assess the efficacy of liposomes for the rescue of bone loss in rats. (b) Three-dimensional micro-CT images of distal femurs from each group. (c) Quantitative analysis of BMD (g/cm^3) and Tb.N (1/mm) (n = 6). (d) Representative images of H&E staining of distal femurs from each group. (e) Calcein double labeling of dynamic trabecular bone and (f) histomorphometric analyses.

https://doi.org/10.1021/acsnano.5c05460
ACS Nano 2025, 19, 23955−23968

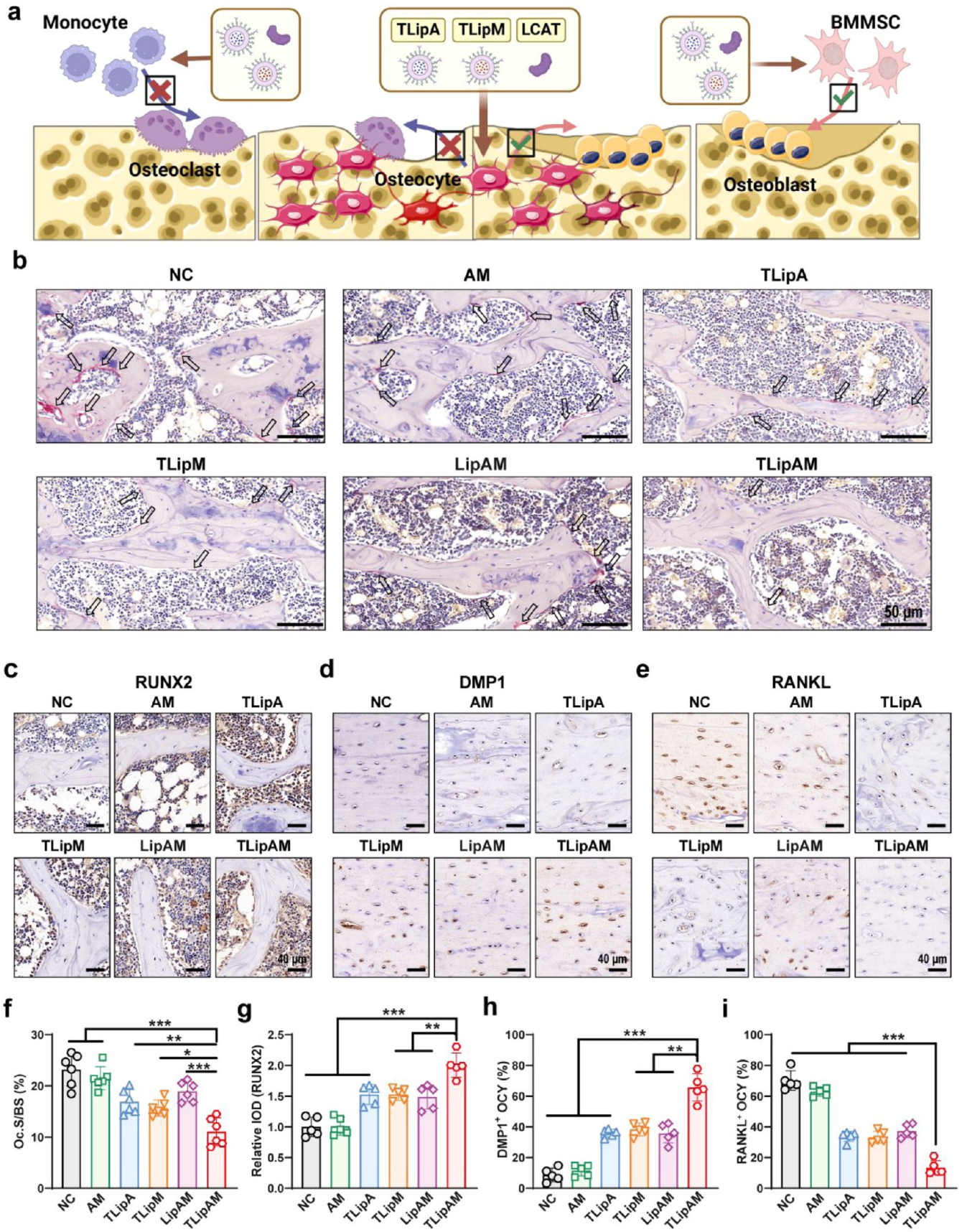

Figure 6. (a) Schematic diagram showing the effect of TLipAM and LCAT on the improvement of bone formation and reduction of osteoclast activity in BMMSCs, monocytes, and osteocytes *in vivo*. (b) TRAP staining images of distal femurs from each group. Scale bars are 50 μm. (c) RUNX2 immunohistochemistry of distal femurs from each group. Scale bars are 40 μm. DMP1 (d) and RANKL (e)

https://doi.org/10.1021/acsnano.5c05460
ACS Nano 2025, 19, 23955−23968

Figure 6. continued

immunohistochemical staining images in the distal femur cortical bone matrix. Scale bars are 40 μm. (f) Quantification of TRAP Oc.S/BS., (g) RUNX2 intensity, (h) DMP1$^+$ cells, and (i) and RANKL$^+$ cells of distal femurs from each group (n = 5).

siLCAT HCM). The experimental results found that the effect of LipAM + siLCAT HCM on the promotion of osteogenic differentiation was inhibited by the silencing of LCAT in hepatocytes (Figures 4b,c and S17−S19). As for osteoclast differentiation, LipAM + siLCAT HCM showed a higher osteoclast differentiation induction ability compared to LipAM and siNC HCM (Figures 4d−g and S20). Additionally, silencing LCAT caused a shift from osteogenic differentiation induction to osteoclast differentiation promotion (Figures 4h,i and S21−S24). Therefore, LipAM HCM was shown to promote osteogenic differentiation and inhibit osteoclast differentiation, and the function of LipAM HCM was eliminated following the silencing of LCAT in hepatocytes. The pro-osteogenic and antiosteoclast functions exerted by LipAM HCM were mediated through the secretion of LCAT.

Rescue of Bone Loss in OVX Rats. Animal experiments were performed to evaluate the function of TLipAM in treating postmenopausal osteoporosis. In ovariectomized (OVX) rats, pharmacological interventions were initiated 4 weeks post-operatively via intraperitoneal injections administered every 3 days (10 administrations over 30 days). Tissues at post-operative week 9 were collected for analysis via micro-computed tomography (micro-CT), hematoxylin-eosin (H&E) staining, immunohistochemistry (IHC), and TRAP staining. Additionally, a calcein double-labeling experiment was conducted prior to euthanasia (Figure 5a). Micro-CT analysis provided a detailed assessment of the distal femur, including trabecular bone mineral density (BMD), trabecular number (Tb.N), bone volume per tissue volume (BV/TV), cortical and trabecular thickness (Tb.Th), bone surface-to-volume ratio (BS/BV), and trabecular separation (Tb.Sp). These parameters allowed for a comprehensive evaluation of bone mass, cortical thickness, and trabecular structure. The results of BMD indicated that injections of free arginine and active ingredient did not significantly improve the porous bone structure (NC 1.24 ± 0.23 and AM 1.27 ± 0.22). In contrast, TLipA (2.00 ± 0.21) and TLipM (2.06 ± 0.21) demonstrated therapeutic effects on bone mass and microarchitecture, consistent with *in vitro* findings. LipAM (1.87 ± 0.25) showed modest bone repair effects compared with the OVX group. In contrast, TLipAM exhibited the most pronounced therapeutic effect (3.20 ± 0.50) (Figures 5b,c and S25). In addition, after 1 month of treatment, safety assessments of the liver and serum of the rats were examined, where no significant hepatotoxicity or side effects were observed (Figure S26).

H&E staining showed increased trabecular density in groups treated with TLipA and TLipM, while free arginine and active ingredient had no measurable impact on bone structure. The results were consistent with the findings from the micro-CT tests. The therapeutic effects of TLipA and TLipM were attributed to their combined actions on osteoblasts,osteoclasts, and osteocytes, as well as their promotion of LCAT secretion through the liver-bone axis. While LipAM exhibited some bone repair effects, its limited efficacy compared to TLipAM was likely due to its weak bone-targeting capacity. TLipAM demonstrated superior bone mass recovery, making it the most effective treatment among the tested options (Figure 5d). Therefore, TLipAM effectively alleviated bone mass loss in OVX rats, outperforming LipAM and the free agents. Its enhanced efficacy can be attributed to its targeted bone delivery and ability to modulate bone remodeling processes through systemic and local mechanisms.

Osteoclastogenesis and Osteogenesis in OVX Rats. The calcein double-labeling experiment could show the speed of bone formation. The mineral apposition rate (MAR) increased with the use of TLipA and TLipM, and the TLipAM group achieved the strongest effect on bone formation. It is noteworthy that the LipAM group still had a certain effect in promoting bone formation, which indicated that the increase in LCAT levels promoted by LipAM through the liver had a certain effect on bone promotion (Figure 5e,f).

The effects of TLipAM on enhancing bone formation and reducing osteoclast activity in BMMSCs, monocytes, and osteocytes are summarized in Figure 6a. TRAP staining on the tissue sections was performed to measure the effects of different treatments on the osteoclast activity of OVX mice. Multinucleated osteoclast number/bone surface (N.Oc/BS) and osteoclast surface per bone surface (Oc.S/BS) of TRAP staining were analyzed to show the number and area of osteoclasts (Figures 6b,f and S27). The osteoclast genesis was significantly inhibited after the treatments with TLipA, TLipM, and LipAM groups, where TLipAM groups showed the most inhibition effect. For assessing osteogenesis, IHC was used to detect expression of RUNX2, BMP2, and COL1. Contrary to the negligible effect of arginine on osteogenesis observed *in vitro*, the expression of osteogenic differentiation genes in the TLipA group of mice remained relatively high. This paradoxical *in vivo* efficacy may be attributed to the synergistic actions of the secretion of LCAT from the liver and regulation of osteocytes of TLipA. The results confirmed that the osteogenic differentiation activation of osteoblasts in the TLipAM group achieved the best effect of promoting osteogenesis and suppressing osteoclastogenesis (Figures 6c,g, S28, and S29).

Analysis of osteocyte-related markers further demonstrated a reduction in the expression of RANKL and DKK1, associated with osteoclast function regulation, while the expression of DMP1, OPG, and β-catenin, which are related to osteogenic function regulation, was significantly increased (Figure 6d,e,h,i and S30−S32). These results indicated that TLipAM not only targeted bone but also modulated systemic factors, including hepatocyte-mediated LCAT production, to restore bone balance and counteract osteoporosis. TLipAM demonstrated superior efficacy in promoting bone formation, inhibiting bone resorption, and restoring bone homeostasis through its dual mechanisms of targeted bone delivery and systemic regulation. These findings suggest that TLipAM provides significant clinical potential for improving bone health and treating osteoporosis.

CONCLUSIONS

In summary, we developed an ALN-functionalized liposomal system loaded with arginine and active ingredient for osteoporosis therapy. The target liposomes directly modulated BMMSCs,osteoclasts, and osteocytes to promote osteogenesis while

https://doi.org/10.1021/acsnano.5c05460
ACS Nano 2025, 19, 23955−23968

suppressing bone resorption. Meanwhile, the nonspecific hepatic accumulation of liposomes enhanced LCAT secretion. We demonstrated that LCAT promoted osteogenesis and inhibited osteoclastogenesis via the liver-bone axis, thereby repurposing the nontargeted drug fraction retained in liver. Through *in vivo* and *in vitro* validation, this dual-pathway mechanism was confirmed to synergistically enhance osteoanabolic effects and inhibit osteoclastogenesis, achieving significant therapeutic efficacy in osteoporosis models. The reported approach maximizes the bioavailability of nanomedicines and holds significant implications for the advancement of osteoporosis treatments. This work provides an avenue for leveraging physiological organ interactions to amplify nanotherapeutic precision, with broad implications for treating osteoporosis and other multisystem disorders.

EXPERIMENTAL SECTION

Preparation of Liposomes. DSPE-PEG2000-ALN was synthesized via an amidation reaction between DSPE-PEG2000-NHS and ALN. Briefly, 1 g of DSPE-PEG2000-NHS was added to an ALN solution containing 307.5 mg of 4-(4,6-dimethoxy-1,3,5-triazin-2-yl)-4-methylmorpholinium chloride hydrate (DMTMM) and stirred at 500 rpm for 12 h. The resulting mixture was dialyzed against deionized water for 2 days and subsequently freeze-dried to obtain DSPE-PEG2000-ALN. The final yield of PEG-ALN was 83.2%.

TLipM was prepared by using a film-dispersion method. In brief, DPPC (300 mg), Chol (100 mg), and DSPE-PEG2000-ALN (100 mg) were dissolved in 50 mL of chloroform in a 500 mL flask and evaporated under reduced pressure to form a thin lipid film. The film was then rehydrated by adding 6 mL of phosphate-buffered saline (PBS) buffer (10 mM) containing 500mg of active ingredient with ultrasonication to assist the process. The resulting liposomes were extruded through a high-pressure microfluidizer (NanoGenizer-II, Genizer) four times at an operating pressure of 15,000 psi, followed by purification using a G-50 column to yield TLipM. The loading content of active ingredient is 9.75%. For the preparation of TLipA, active ingredient was replaced with arginine in the formulation. Arginine was quantitatively determined using UV−vis absorption spectroscopy with a mixed solution of naphthol and diacetyl as the color-developing reagent, and the drug loading content was 8.56%. To prepare nontargeted liposomal nanomedicines, DSPE-PEG2000-ALN can simply be substituted with DSPE-mPEG2000.

Targeted and nontargeted liposomes were labeled with DID dye (denoted as TLipDID and LipDID, respectively) to investigate their targeting efficiency toward bone and liver using an *ex vivo* imaging strategy. The distribution of TLipDID and LipDID in major organs and bone was evaluated at 6 and 24 h postinjection.

Promotion of Bone Osteogenesis. The osteoblastogenesis medium was supplemented with 10 mM β-glycerophosphate, 10 nM active ingredient, and 50 μg/mL ascorbic acid. RAW 264.7 cells were stimulated with 50 ng/mL RANKL for 6 days. Osteoclasts were stained by using the TRAP staining kit (Sigma-Aldrich, 387A-1KT). Related indexes of MLO-Y4 were detected after our nanomedicine stimulation for 7 days. We used the stimulation concentration of arginine to be 400 μM, and the stimulation concentration of active ingredient was 10 μM. The arginine-to-active ingredient molar ratio was precisely maintained at 40:1.

ELISA Assays. ELISA assays were conducted for LCAT and IGF-1 of serum and LCAT of bone marrow *in vivo* after 24 h of tail vein injection. Conditional medium of hepatocytes *in vitro* was acquired after 24 h of LipAM stimulation. The cytokines produced by AML12, BMMSCs, RAW 264.7, MLO-Y4 cells, and serum bone marrow after the stimulation of different liposomes were determined by specific ELISA kits following the manufacturer's instructions.

Preparation of HCM. Supernatants of AML12 treated with different liposomes for 2 days extracts were collected and centrifuged at ×1000*g* for 5 min. The supernatants were further filtered with a 0.22 μm filter and mixed with fresh medium in a proportion of 1:1 to obtain HCM. HCM was used to replace the medium of BMMSCs, RAW 264.7, and MLO-Y4 cells for further cultivation.

siRNA Transfection. SiRNA targeting siLCAT and scrambled siRNA (GenePharma) were diluted with DEPC water. 100 pmol of siRNA and 5 μL of Lipofectamine 2000 (11668019; Thermo Fisher Scientific) were added to 250 μL of Opti-MEM I (31985070; Thermo Fisher Scientific). For transfection, the culture medium was replaced with Opti-MEM I, and the transfection mixture was added.

OVX Rat Model. OVX were performed on 8-week-old female rats under general anesthesia, and both ovaries were excised under sterile conditions. The nanomedicines were quantified using the amounts of arginine (6 mg/mL) and active ingredient(6 mg/mL) encapsulation. Each injection is 500 μL of arginine and 500 μL of active ingredientfo r a total of 1 mL of liquid.

Ethics Statement. The experiments were approved by the Medical Ethics Committee of the Qilu Hospital of Shandong University (approval No. DWLL-202400157). Liposome injection was administered through the tail vein.

Statistical Analysis. One-way analysis of variance (ANOVA) was employed for comparisons between groups. All the data were expressed as mean ± standard deviation (SD). Statistical significance was set at $P < 0.05$.

ASSOCIATED CONTENT

Supporting Information

The Supporting Information is available free of charge at https://pubs.acs.org/doi/10.1021/acsnano.5c05460.

Materials; characterization methods; and detailed experimental methods *in vitro* (cell culture, ALP, ARS staining, qPCR, Western blotting, immunofluorescence and osteoclastogenesis assays) and *in vivo* (animal models, Micro-CT, bone histomorphometry, immunohistochemistry and bone dynamic labeling) (PDF)

AUTHOR INFORMATION

Corresponding Authors

Lianlei Wang − *Department of Orthopedics, Qilu Hospital of Shandong University, Jinan, Shandong 250014, China*; Email: wllspine@163.com

Zhiliang Gao − *Department of Orthopedics, Qilu Hospital of Shandong University, Jinan, Shandong 250014, China; Shandong Key Laboratory of Magnetic Field-Free Medicine & Functional Imaging, Research Institute of Magnetic Field-free Medicine & Functional Imaging, National Medicine-Engineering Interdisciplinary Industry-Education Integration Innovation Platform, Shandong University, Jinan, Shandong 250012, China*; orcid.org/0009-0003-5256-3497; Email: zlgao@email.sdu.edu.cn

Jiwei Cui − *Key Laboratory of Colloid and Interface Chemistry of the Ministry of Education, School of Chemistry and Chemical Engineering and Shandong Key Laboratory of Targeted Drug Delivery and Advanced Pharmaceutics, Shandong University, Jinan, Shandong 250100, China*; orcid.org/0000-0003-1018-4336; Email: jwcui@sdu.edu.cn

Xinyu Liu − *Department of Orthopedics, Qilu Hospital of Shandong University, Jinan, Shandong 250014, China*; Email: xyliu@email.sdu.edu.cn

Authors

Yunhao You − *Department of Orthopedics, Qilu Hospital of Shandong University, Jinan, Shandong 250014, China*

Shaoqiu Leng − *Department of Hematology, Qilu Hospital of Shandong University, Jinan, Shandong 250014, China*

https://doi.org/10.1021/acsnano.5c05460
ACS Nano 2025, 19, 23955−23968

Jie Shi − *Department of Orthopedics, Qilu Hospital of Shandong University, Jinan, Shandong 250014, China*
Han Yang − *Key Laboratory of Colloid and Interface Chemistry of the Ministry of Education, School of Chemistry and Chemical Engineering, Shandong University, Jinan, Shandong 250100, China*
Mingzheng Chang − *Department of Orthopedics, Qilu Hospital of Shandong University, Jinan, Shandong 250014, China*
Qingliang Ma − *Department of Orthopedics, Qilu Hospital of Shandong University, Jinan, Shandong 250014, China*
Dapeng Zhang − *Department of Orthopedics, Qilu Hospital of Shandong University, Jinan, Shandong 250014, China*
Haochen Sun − *Department of Orthopedics, Qilu Hospital of Shandong University, Jinan, Shandong 250014, China*

Complete contact information is available at: https://pubs.acs.org/10.1021/acsnano.5c05460

Author Contributions

#Y.Y., S.L., and J.S. contributed equally to this work.

Notes

The authors declare no competing financial interest.

ACKNOWLEDGMENTS

This work was supported by the National Key R&D Program of China (2023YFC2509700), National Natural Science Foundation of China (22372091 and U24A20670), and Natural Science Foundation of Shandong Province of China (ZR2024QB267). This work was performed in part at the Analytical Centre for Structural Constituent and Physical Property, and the Translational Medicine Core Facility of Advanced Medical Research Institute at Shandong University.

REFERENCES

(1) Kim, H.; Lee, K.; Kim, J. M.; Kim, M. Y.; Kim, J. R.; Lee, H. W.; Chung, Y. W.; Shin, H. I.; Kim, T.; Park, E. S.; Rho, J.; Lee, S. H.; Kim, N.; Lee, S. Y.; Choi, Y.; Jeong, D. Selenoprotein W Ensures Physiological Bone Remodeling by Preventing Hyperactivity of Osteoclasts. *Nat. Commun.* **2021**, *12* (1), No. 2258.
(2) You, Y.; Liu, J.; Zhang, L.; Li, X.; Sun, Z.; Dai, Z.; Ma, J.; Jiao, G.; Chen, Y. WTAP-Mediated m(6)A Modification Modulates Bone Marrow Mesenchymal Stem Cells Differentiation Potential and Osteoporosis. *Cell Death Dis.* **2023**, *14* (1), No. 33.
(3) Zheng, Y.; Zhang, Z.; Fu, Z.; Fan, A.; Song, N.; Wang, Q.; Fan, S.; Xu, J.; Xiang, J.; Liu, X. Oral Propolis Nanoemulsions Modulate Gut Microbiota to Balance Bone Remodeling for Enhanced Osteoporosis Therapy. *ACS Nano* **2024**, *18* (38), 26153−26167.
(4) Ye, J.; Jiang, J.; Zhou, Z.; Weng, Z.; Xu, Y.; Liu, L.; Zhang, W.; Yang, Y.; Luo, J.; Wang, X. Near-Infrared Light and Upconversion Nanoparticle Defined Nitric Oxide-Based Osteoporosis Targeting Therapy. *ACS Nano* **2021**, *15* (8), 13692−13702.
(5) He, C.; He, P.; Ou, Y.; Tang, X.; Wei, H.; Xu, Y.; Bai, S.; Guo, Z.; Hu, R.; Xiong, K.; Du, G.; Sun, X. Rectifying the Crosstalk between the Skeletal and Immune Systems Improves Osteoporosis Treatment by Core−Shell Nanocapsules. *ACS Nano* **2025**, *19* (5), 5549−5567.
(6) Ma, W.; Wang, F.; You, Y.; Wu, W.; Chi, H.; Jiao, G.; Zhang, L.; Zhou, H.; Wang, H.; Chen, Y. Ortho-Silicic Acid Inhibits RANKL-Induced Osteoclastogenesis and Reverses Ovariectomy-Induced Bone Loss In Vivo. *Biol. Trace Elem. Res.* **2021**, *199* (5), 1864−1876.
(7) Zhang, Q. Y.; Gong, H. B.; Jiang, M. Y.; Jin, F.; Wang, G.; Yan, C. Y.; Luo, X.; Sun, W. Y.; Ouyang, S. H.; Wu, Y. P.; Duan, W. J.; Liang, L.; Cao, Y. F.; Sun, X. X.; Liu, M.; Jiao, G. L.; Wang, H. J.; Hiroshi, K.; Wang, X.; He, R. R.; Li, Y. F. Regulation of Enzymatic Lipid Peroxidation in Osteoblasts Protects against Postmenopausal Osteoporosis. *Nat. Commun.* **2025**, *16* (1), No. 758.
(8) Alhashmi, M.; Gremida, A. M. E.; Maharana, S. K.; Antonaci, M.; Kerr, A.; Fu, S.; Lunn, S.; Turner, D. A.; Al-Maslamani, N. A.; Liu, K.; Meschis, M. M.; Sutherland, H.; Wilson, P.; Clegg, P.; Wheeler, G. N.; van 't Hof, R. J.; Bou-Gharios, G.; Yamamoto, K. Skeletal Progenitor LRP1 Deficiency Causes Severe and Persistent Skeletal Defects with Wnt Pathway Dysregulation. *Bone Res.* **2025**, *13* (1), No. 17.
(9) Alonso, N.; Albagha, O. M. E.; Azfer, A.; Larraz-Prieto, B.; Berg, K.; Riches, P. L.; Ostanek, B.; Kocjan, T.; Marc, J.; Langdahl, B. L.; Ralston, S. H. Genome-Wide Association Study Identifies Genetic Variants Which Predict the Response of Bone Mineral Density to Teriparatide Therapy. *Ann. Rheum. Dis.* **2023**, *82* (7), 985−991.
(10) Qaseem, A.; Hicks, L. A.; Etxeandia-Ikobaltzeta, I.; Shamliyan, T.; Cooney, T. G.; Cross, J. T.; Fitterman, N.; Lin, J. S.; Maroto, M.; Obley, A. J.; Tice, J. A.; Tufte, J. E. Pharmacologic Treatment of Primary Osteoporosis or Low Bone Mass to Prevent Fractures in Adults: A Living Clinical Guideline From the American College of Physicians. *Ann. Int. Med.* **2023**, *176* (2), 224−238.
(11) Yao, Z.; Ayoub, A.; Srinivasan, V.; Wu, J.; Tang, C.; Duan, R.; Milosavljevic, A.; Xing, L.; Ebetino, F. H.; Frontier, A. J.; Boyce, B. F. active ingredient and a Low Antiresorptive Activity Bisphosphonate Conjugate Prevent and Reverse Ovariectomy-Induced Bone Loss in Mice through Dual Antiresorptive and Anabolic Effects. *Bone Res.* **2024**, *12* (1), No. 52.
(12) Ding, P.; Gao, C.; Zhou, J.; Mei, J.; Li, G.; Liu, D.; Li, H.; Liao, P.; Yao, M.; Wang, B.; Lu, Y.; Peng, X.; Jiang, C.; Yin, J.; Huang, Y.; Zheng, M.; Gao, Y.; Zhang, C.; Gao, J. Mitochondria from Osteolineage Cells Regulate Myeloid Cell-Mediated Bone Resorption. *Nat. Commun.* **2024**, *15* (1), No. 5094.
(13) Ma, W.; Lu, H.; Xiao, Y.; Wu, C. Advancing Organoid Development with 3D Bioprinting. *Organoid Res.* **2025**, *1* (1), No. 025040004.
(14) Bai, L.; Song, P.; Su, J. Bioactive Elements Manipulate Bone Regeneration. *Biomater. Transl.* **2023**, *4* (4), 248−269.
(15) Lin, C.-H.; Srioudom, J. R.; Sun, W.; Xing, M.; Yan, S.; Yu, L.; Yang, J. The Use of Hydrogel Microspheres as Cell and Drug Delivery Carriers for Bone, Cartilage, and Soft Tissue Regeneration. *Biomater. Transl.* **2024**, *5* (3), 236−256.
(16) Song, S.; Zhang, J.; Fang, Y.; Li, W.; Zeng, H.; Fang, Z.; Wang, T.; Xie, Y.; Liu, C.; Wang, J. Nerve−Bone Crosstalk Manipulates Bone Organoid Development and Bone Regeneration: A Review and Perspectives. *Organoid Res.* **2025**, *1* (1), No. 8294.
(17) Chu, W.; Peng, W.; Lu, Y.; Liu, Y.; Li, Q.; Wang, H.; Wang, L.; Zhang, B.; Liu, Z.; Han, L.; Ma, H.; Yang, H.; Han, C.; Lu, X. PRMT6 Epigenetically Drives Metabolic Switch from Fatty Acid Oxidation toward Glycolysis and Promotes Osteoclast Differentiation During Osteoporosis. *Adv. Sci.* **2024**, *11* (40), No. e2403177.
(18) Deng, A.-F.; Wang, F.-X.; Wang, S.-C.; Zhang, Y.-Z.; Bai, L.; Su, J.-C. Bone-Organ Axes: Bidirectional Crosstalk. *Mil. Med. Res.* **2024**, *11* (1), No. 37.
(19) Lin, L.; Guo, Z.; He, E.; Long, X.; Wang, D.; Zhang, Y.; Guo, W.; Wei, Q.; He, W.; Wu, W.; Li, J.; Wo, L.; Hong, D.; Zheng, J.; He, M.; Zhao, Q. SIRT2 Regulates Extracellular Vesicle-Mediated Liver-Bone Communication. *Nat. Metab.* **2023**, *5* (5), 821−841.
(20) Lu, K.; Shi, T.-S.; Shen, S.-Y.; Shi, Y.; Gao, H.-L.; Wu, J.; Lu, X.; Gao, X.; Ju, H.; Wang, W.; Cao, Y.; Chen, D.; Li, C.-J.; Xue, B.; Jiang, Q. Defects in a Liver-Bone Axis Contribute to Hepatic Osteodystrophy Disease Progression. *Cell Metab.* **2022**, *34* (3), 441−457.
(21) Ullah, A.; Chen, Y.; Singla, R. K.; Cao, D.; Shen, B. Exploring Cytokines Dynamics: Uncovering Therapeutic Concepts for Metabolic Disorders in Postmenopausal Women- Diabetes, Metabolic Bone Diseases, and Non-Alcohol Fatty Liver Disease. *Ageing Res. Rev.* **2024**, *101*, No. 102505.
(22) Vachliotis, I. D.; Anastasilakis, A. D.; Rafailidis, V.; Polyzos, S. A. Osteokines in Nonalcoholic Fatty Liver Disease. *Curr. Obes. Rep.* **2024**, *13* (4), 703−723.
(23) Chen, Z.; Wang, S. P.; Krsmanovic, M. L.; Castro-Perez, J.; Gagen, K.; Mendoza, V.; Rosa, R.; Shah, V.; He, T.; Stout, S. J.;

Geoghagen, N. S.; Lee, S. H.; McLaren, D. G.; Wang, L.; Roddy, T. P.; Plump, A. S.; Hubbard, B. K.; Sinz, C. J.; Johns, D. G. Small Molecule Activation of Lecithin Cholesterol Acyltransferase Modulates Lipoprotein Metabolism in Mice and Hamsters. *Metabolism* **2012**, *61* (4), 470−481.
(24) Jia, F.; Ruan, L.; Du, C.; Liu, Y.; Cai, X.; Dou, R.; Zhang, J.; Liu, X.; Chen, J.; Zhang, X.; Chai, Z.; Hu, Y. The Nanoformula of active ingredient Acid and Calcium Carbonate Targets Osteoclasts and Reverses Osteoporosis. *Biomaterials* **2023**, *296*, No. 122059.
(25) Sun, W.; Wang, H.; Qi, Y.; Li, M.; Zhang, R.; Gao, Z.; Cui, J.; Yu, D. Metal-Phenolic Vehicles Potentiate Cycle-Cascade Activation of Pyroptosis and cGAS-STING Pathway for Tumor Immunotherapy. *ACS Nano* **2024**, *18* (34), 23727−23740.
(26) Yu, B.; Gao, Q.; Sheng, S.; Zhou, F.; Geng, Z.; Wei, Y.; Zhang, H.; Hu, Y.; Wang, S.; Huang, J.; Li, M.; Su, J. Smart Osteoclasts Targeted Nanomedicine Based on Amorphous $CaCO_3$ for Effective Osteoporosis Reversal. *J. Nanobiotechnol.* **2024**, *22* (1), No. 153.
(27) Omo-Lamai, S.; Zamora, M. E.; Patel, M. N.; Wu, J.; Nong, J.; Wang, Z.; Peshkova, A.; Majumder, A.; Melamed, J. R.; Chase, L. S.; Essien, E.-O.; Weissman, D.; Muzykantov, V. R.; Marcos-Contreras, O. A.; Myerson, J. W.; Brenner, J. S. Physicochemical Targeting of Lipid Nanoparticles to the Lungs Induces Clotting: Mechanisms and Solutions. *Adv. Mater.* **2024**, *36* (26), No. 2312026.
(28) Liu, X.; Li, F.; Dong, Z.; Gu, C.; Mao, D.; Chen, J.; Luo, L.; Huang, Y.; Xiao, J.; Li, Z.; Liu, Z.; Yang, Y. Metal-polyDNA Nanoparticles Reconstruct Osteoporotic Microenvironment for Enhanced Osteoporosis Treatment. *Sci. Adv.* **2023**, *9* (31), No. eadf3329.
(29) Chen, Y.; Chen, Q. W.; Fu, F. S.; Gu, H. Y.; Yu, A.; Zhang, X. Z. Bone Destruction-Chemotactic Osteoprogenitor Cells Deliver Liposome Nanomedicines for the Treatment of Osteosarcoma and Osteoporosis. *ACS Nano* **2024**, *18* (43), 29864−29879.
(30) Luo, Z.; Lu, Y.; Shi, Y.; Jiang, M.; Shan, X.; Li, X.; Zhang, J.; Qin, B.; Liu, X.; Guo, X.; Huang, J.; Liu, Y.; Wang, S.; Li, Q.; Luo, L.; You, J. Neutrophil Hitchhiking for Drug Delivery to the Bone Marrow. *Nat. Nanotechnol.* **2023**, *18* (6), 647−656.
(31) Ngo, W.; Ahmed, S.; Blackadar, C.; Bussin, B.; Ji, Q.; Mladjenovic, S. M.; Sepahi, Z.; Chan, W. C. W. Why Nanoparticles Prefer Liver Macrophage Cell Uptake in Vivo. *Adv. Drug Delivery Rev.* **2022**, *185*, No. 114238.
(32) Jayaraman, M.; Ansell, S. M.; Mui, B. L.; Tam, Y. K.; Chen, J.; Du, X.; Butler, D.; Eltepu, L.; Matsuda, S.; Narayanannair, J. K.; Rajeev, K. G.; Hafez, I. M.; Akinc, A.; Maier, M. A.; Tracy, M. A.; Cullis, P. R.; Madden, T. D.; Manoharan, M.; Hope, M. J. Maximizing the Potency of siRNA Lipid Nanoparticles for Hepatic Gene Silencing In Vivo. *Angew. Chem., Int. Ed.* **2012**, *51* (34), 8529−8533.
(33) Gao, Z.; Wang, N.; Ma, Y.; Sun, H.; Li, M.; Dai, Y.; Jiang, X.; Ni, S.; Hao, J.; Cui, J. Targeting Neutrophils Potentiates Hitchhiking Delivery of Drugs and Agonists for Postsurgical Chemo-Immunotherapy. *Nano Today* **2024**, *54*, No. 102096.
(34) Gao, Z.; Sun, H.; Yang, S.; Li, M.; Qi, N.; Cui, J. Red Blood Cell-Like Poly(ethylene glycol) Particles: Influence of Particle Stiffness on Biological Behaviors. *ACS Macro Lett.* **2024**, *13* (8), 966−971.
(35) Wang, L.; Zhang, G.; Sun, Y.; Wu, Z.; Ren, C.; Zhang, Z.; Peng, X.; Zhang, Y.; Zhao, Y.; Li, C.; Gao, L.; Liang, X.; Sun, H.; Cui, J.; Ma, C. Enhanced Delivery of TLR7/8 Agonists by Metal-Organic Frameworks for Hepatitis B Virus Cure. *ACS Appl. Mater. Interfaces* **2022**, *14* (41), 46176−46187.
(36) Chang, W.; Tian, B.; Qin, Q.; Li, D.; Zhang, Y.; Zhou, C.; Wu, B.; Zhang, M.; Shan, H.; Ni, Y.; Dong, Q.; Wang, C.; Zhou, X.-Z.; Bai, J. Receptor Activator of Nuclear Factor Kappa-B-Expressing Mesenchymal Stem Cells-Derived Extracellular Vesicles for Osteoporosis Therapy. *ACS Nano* **2024**, *18* (52), 35368−35382.
(37) Böttger, R.; Pauli, G.; Chao, P.-H.; Al Fayez, N.; Hohenwarter, L.; Li, S.-D. Lipid-Based Nanoparticle Technologies for Liver Targeting. *Adv. Drug Delivery Rev.* **2020**, *154-155* (155), 79−101.
(38) Witzigmann, D.; Kulkarni, J. A.; Leung, J.; Chen, S.; Cullis, P. R.; Van Der Meel, R. Lipid Nanoparticle Technology for Therapeutic Gene Regulation in the Liver. *Adv. Drug Delivery Rev.* **2020**, *159*, 344−363.
(39) Nelson, A. L.; Mancino, C.; Gao, X.; Choe, J. A.; Chubb, L.; Williams, K.; Czachor, M.; Marcucio, R.; Taraballi, F.; Cooke, J. P.; Huard, J.; Bahney, C.; Ehrhart, N. *β*-Catenin mRNA Encapsulated in SM-102 Lipid Nanoparticles Enhances Bone Formation in a Murine Tibia Fracture Repair Model. *Bioact. Mater.* **2024**, *39*, 273−286.
(40) Yang, X.; Fan, Y.; Liang, J.; Cao, R.; Zhang, B.; Li, J.; Li, Z.; He, S.; Liu, N.; Du, J.; Hu, Y. Polyaptamer-Driven Crystallization of active ingredient for Synergistic Osteoporosis Treatment through Osteoclastic Inhibition and Osteogenic Promotion. *ACS Nano* **2024**, *18* (33), 22431−22443.
(41) Dilliard, S. A.; Siegwart, D. J. Passive, Active and Endogenous Organ-Targeted Lipid and Polymer Nanoparticles for Delivery of Genetic Drugs. *Nat. Rev. Mater.* **2023**, *8* (4), 282−300.
(42) Zhang, Y.; Higgins, C. B.; Van Tine, B. A.; Bomalaski, J. S.; DeBosch, B. J. Pegylated Arginine Deiminase Drives Arginine Turnover and Systemic Autophagy to Dictate Energy Metabolism. *Cell Rep. Med.* **2022**, *3* (1), No. 100498.
(43) Wang, D.; Cai, J.; Pei, Q.; Yan, Z.; Zhu, F.; Zhao, Z.; Liu, R.; Guo, X.; Sun, T.; Liu, J.; Tian, Y.; Liu, H.; Shao, X.; Huang, J.; Hao, X.; Chang, Q.; Luo, Z.; Jing, D. Gut Microbial Alterations in Arginine Metabolism Determine Bone Mechanical Adaptation. *Cell Metab.* **2024**, *36* (6), 1252−1268.e8.
(44) Anurag, P.; Anuradha, C. V. active ingredient Improves Lipid Metabolism and Attenuates Lipid Peroxidation in High Fructose-Fed Rats. *Diabetes, Obes. Metab.* **2002**, *4* (1), 36−42.
(45) Xie, X.; Hu, L.; Mi, B.; Xue, H.; Hu, Y.; Panayi, A. C.; Endo, Y.; Chen, L.; Yan, C.; Lin, Z.; Li, H.; Zhou, W.; Liu, G. active ingredient Alleviates Bone Loss in Ovariectomized Mice through Inhibition of Autophagy of Osteoclast Precursors Mediated by E2F1. *Cell Commun. Signaling* **2022**, *20* (1), No. 165.
(46) Yang, K.; Wang, X.; Zhang, C.; Liu, D.; Tao, L. active ingredient Improves HPRT1-Targeted Purine Metabolism and Repairs NR4A1-Mediated Autophagic Flux by Modulating FoxO1 Nucleocytoplasmic Shuttling to Treat Postmenopausal Osteoporosis. *Cell Death Dis.* **2024**, *15* (11), No. 795.
(47) Cui, J.; Shibata, Y.; Zhu, T.; Zhou, J.; Zhang, J. Osteocytes in Bone Aging: Advances, Challenges, and Future Perspectives. *Ageing Res. Rev.* **2022**, *77*, No. 101608.
(48) He, W.; Wang, M.; Zhang, X.; Wang, Y.; Zhao, D.; Li, W.; Lei, F.; Peng, M.; Zhang, Z.; Yuan, Y.; Huang, Z. Estrogen Induces LCAT to Maintain Cholesterol Homeostasis and Suppress Hepatocellular Carcinoma Development. *Cancer Res.* **2024**, *84* (15), 2417−2431.
(49) Zaidi, M.; Yuen, T.; Iqbal, J. Reverse Cholesterol Transport and Hepatic Osteodystrophy. *Cell Metab.* **2022**, *34* (3), 347−349.
(50) Ma, T.; Tian, X.; Zhang, B.; Li, M.; Wang, Y.; Yang, C.; Wu, J.; Wei, X.; Qu, Q.; Yu, Y.; Long, S.; Feng, J. W.; Li, C.; Zhang, C.; Xie, C.; Wu, Y.; Xu, Z.; Chen, J.; Yu, Y.; Huang, X.; He, Y.; Yao, L.; Zhang, L.; Zhu, M.; Wang, W.; Wang, Z. C.; Zhang, M.; Bao, Y.; Jia, W.; Lin, S. Y.; Ye, Z.; Piao, H. L.; Deng, X.; Zhang, C. S.; Lin, S. C. Low-Dose active ingredient Targets the Lysosomal AMPK Pathway through PEN2. *Nature* **2022**, *603* (7899), 159−165.
(51) Ma, A.; Wang, J.; Yang, L.; An, Y.; Zhu, H. AMPK Activation Enhances the Anti-Atherogenic Effects of High Density Lipoproteins in apoE$^{-/-}$ Mice. *J. Lipid Res.* **2017**, *58* (8), 1536−1547.
(52) Manochantr, S.; Meesuk, L.; Chadee, N.; Suwanprateeb, J.; Tantrawatpan, C.; Kheolamai, P. Improvement of Osteogenic Differentiation Potential of Placenta-Derived Mesenchymal Stem Cells by active ingredient via AMPK Pathway Activation. *Stem Cell Res.Ther.* **2024**, *15* (1), No. 417.
(53) Cao, S.; Li, Y.; Song, R.; Meng, X.; Fuchs, M.; Liang, C.; Kachler, K.; Meng, X.; Wen, J.; Schlötzer-Schrehardt, U.; Taudte, V.; Gessner, A.; Kunz, M.; Schleicher, U.; Zaiss, M. M.; Kastbom, A.; Chen, X.; Schett, G.; Bozec, A. L-Arginine Metabolism Inhibits Arthritis and Inflammatory Bone Loss. *Ann. Rheum. Dis.* **2024**, *83* (1), 72−87.

https://doi.org/10.1021/acsnano.5c05460
ACS Nano 2025, 19, 23955−23968